PARP dependent acetylation of N4-cytidine in RNA appeared in UV-damaged chromatin

Alena Kovaříková Svobodová
Department of Molecular Cytology and Cytometry, Institute of Biophysics, Academy of Sciences of the Czech Republic

Lenka Stixová
Department of Molecular Cytology and Cytometry, Institute of Biophysics, Academy of Sciences of the Czech Republic

Aleš Kovařík
Department of Molecular Cytology and Cytometry, Institute of Biophysics, Academy of Sciences of the Czech Republic

Eva Bártová (bartova@ibp.cz)
Department of Molecular Cytology and Cytometry, Institute of Biophysics, Academy of Sciences of the Czech Republic

Research Article

Keywords: RNA acetylation, RNA methylation, histones, DNA repair, PARP, NAT10

Posted Date: October 15th, 2021

DOI: https://doi.org/10.21203/rs.3.rs-971100/v1

Abstract

Posttranscriptional RNA modifications, including the presence of methyl-6-adenosine (m6A), methyl-5-cytosine (m5C), or pseudo-uridine (Ψ), are known for over many years, but their functional properties have not been fully elucidated yet. Similarly, the regulatory role of N4-cytidine (ac4C) acetylation in RNA must be explored. Here, we observed PARP-dependent accumulation of ac4C RNA at UVA-microirradiated chromatin, which appears 2-5 minutes after genome injury, simultaneously with m^6A RNAs but with distinct kinetics. When m^6A RNAs disappeared from the lesions, the high level of ac4C RNA was maintained up to 20 minutes after genome injury. Surprisingly, the process of ac4C RNA accumulation at DNA lesions was not accompanied by the recruitment of acetyltransferase NAT10 to UVA-induced DNA lesions. This process was PARP dependent, and data show how epitranscriptomic features can contribute to DNA damage repair.

Introduction

In general, the acetylation process is a well-described cellular mechanism that regulates gene expression, especially when acetylation appears on the level of histones [1]. However, also N4- acetylcytidine (ac4C), a highly conserved RNA nucleobase, also contributes to the regulation of mRNA stability and translation [2]. On the other hand, information about the function of ac4C RNA in the DNA repair process has not been described yet, but specific histone acetylation was well described at DNA lesions [3]. For instance, we have also observed HDAC1-dependent deacetylation of histone H3 at lysine 9 position at experimentally induced DNA lesions [4], while Meyer et al. (2016) [5] showed that H3K9 acetylation, a pro-activation histone mark, prevents H3K9 methylation; and thus, weakens H3K9me2/3-dependent DNA repair processes. To this fact, Dhar et al. (2017) [6] revised that the histone H4 terminal tails recruit proteins involved in DNA damage repair (DDR), including 53BP1, an important factor of non-homologous end joining (NHEJ) repair. A process mediated by H4 acetylation that provides binding sites for bromodomain proteins, such as ZMYND8 and BRD4, is essential for the repair of double-strand breaks (DSBs) [7, 8]. In addition, Jacquet et al. (2016) [9] showed that acetylation of histone H2A abrogates a pronounced H2A ubiquitination at the same lysine position. A very fundamental observation is that H2A.Z exchange at DSBs, in cooperation with cytochrome P400, leads to acetylation of H4 at damaged chromatin via the function of histone acetyltransferase, Tip60 [10, 11]. Mentioned data showed that histone acetylation regulates not only gene expression but also DNA damage response. In addition to mentioned epigenetic events, here, we test a hypothesis if, and to which extent, ac4C sites in human RNAs play a role in DNA repair processes. We also took into consideration that ac4C RNA is installed in the genome via the function of Nacetyltransferase, NAT10 [12]. The target of the human enzyme NAT10 is preferentially rRNA and tRNA (tRNA-Ser and tRNA-Leu) [13, 14]. To this information, Kudrin et al. (2021) [15] newly identified NOP58 as an ac4C-binding protein, and importantly sirtuin 7 (SIRT7) as a specific ac4C deacetylase. So, taken together, NAT10 can be considered as the essential writer of ac4C on RNA, NOP58 as a reader, while SIRT7 seems to be a highly specific ac4C RNA eraser.

Based on the above-mentioned observation, we addressed a question of how ac4C RNAs contribute to DNA repair machinery and if regulatory protein NAT10 contributes to the process of DNA damage repair. From this view, we additionally tried to reveal in which DNA repair pathways ac4C RNA is involved. We were inspired by the fact that another RNA modification, m^6A, is significantly activated at UV-damaged chromatin [16, 17]. Notably, there was described a non-canonical m^6A-mediated pathway, dependent on the METTL3 and METTL14 enzymes or PARP1/2 proteins [18]. Thus, we also addressed the question if ac4C RNA recruitment to DNA lesions is PARP-dependent. In addition, m^6A-coated mRNA binds to DNA strands to form hybrid DNA-RNA structures that are recognized by m^6A RNA readers, including YTHDF1 and YTHDC1. This process mediates both DSB repair as well nucleotide excision repair (NER) mechanism [19]. From this view, a question remains if ac4C RNAs work in an identical way as m^6A RNAs at DNA lesions.

Materials And Methods

Cell cultivation and Treatment

Mouse embryonic fibroblasts (MEFs) and human breast cancer cell line MCF7 were maintained in Dulbecco's modified Eagle's medium (DMEM) supplemented with 10% fetal bovine serum FCS (Merck, Darmstadt, Germany), penicillin (1 U/ml), and streptomycin (100 µg/ml) at 37°C in a humidified atmosphere containing 5% CO2. For the experiment of dependent recruitment of ac4C on cells cycles, we used HeLa-Fucci cells expressing RFP-Cdt1 in the G1 phase and GFP-geminin in the S/G2/M phases as have previously been described in detail by Sakaue-Sawano et al. (2008) [20]. HeLa-Fucci cells were cultivated in the same *in vitro* conditions.

To inhibit RNA polymerase I and poly ADP ribose polymerase (PARP), at 50% confluence, cells were treated by actinomycin D (#A9415, Merck, Germany), final concentration 0.5 µg/ml, for 2 h, and by Olaparib (#S1060, Selleckchem, Germany), final concentration 10 µM, for 24 h, before microirradiation experiments [21, 22]

To verify the specificity of the antibody, we used treatments by Turbo-DNase (#AM2238, ThermoFisher Scientific, Waltham, MA, USA), Rnase A (#R5503, Merck, Germany), and RNase H (#EN0201, ThermoFisher Scientific, USA). The cells were permeabilized with 0.3% Triton X-100 in PBS for 15 sec, washed twice in phosphate-buffered saline (PBS), and incubated in 300 µl RNase A (1 mg/ml in PBS) or DNase I (7 U in 1x DNase Reaction buffer) or RNase H1 (5U 1x RNase Reaction buffer) for 5 min at 37°C before immunostaining [16, 23].

We observed a significant effect after RNase A treatment. The level of ac4C RNA was reduced in all cells, especially in the nucleolus. After RNase H1 treatment, the fluorescent intensity was only gently reduced in the nucleoplasm. The significant changes were also observed when cells were treated with DNase I, which caused a more diffuse distribution of ac4C RNAs in nuclei of studied cells.

Irradiation by UV light

The cells seeded on 35 mm glass-bottom dishes (#D35-20-1-N, Cellvis Mountain View, CA, USA) and at 50% confluence were sensitized with 10 μM BrdU (#11296736001, Merck, Germany) for 16 h before UVA treatment. The cells were irradiated by the UVA lamps (model GESP-15, 15 W, UVA 330–400 nm wavelength with maximum efficiency at 365 nm) or UVC lamps (Philips, Amsterdam, The Netherlands, model TUV 30 W T8, UVC 254 nm wavelength) for 10 min. After UVC irradiation, the cells were fixed at multiple intervals (5 min, 20 min, 60 min, and 120 min after irradiation). The lamp distance from the sample was 2 cm for the UVA source and 60 cm for the UVC source [17].

Immunofluorescence and confocal microscopy

The immunofluorescence protocol was based on Svobodova et al. (2018) [24] and modified. The cells were fixed with 2 ml 4% paraformaldehyde (PFA; #AAJ19943K2, Fisher Scientific, USA) for 5 min at room temperature (RT), and then 200 ml 1% SDS was added and incubated another 7 min. Afterward, it was permeabilized with 0.2% Triton X-100 for 15 min and washed twice in PBS for 15 min. As a blocking solution, 1% bovine serum albumin (Merck) dissolved in 0.1% 1x PBSTween 20 (BSAT) for 1 hour at RT was used. Dishes with fixed cells were washed for 15 min in PBS and incubated with primary antibodies at a 1:100 dilution in 1% BSAT at 4°C overnight. For immunofluorescence analysis, the following antibodies were used: anti-N4-acetylcytidine/ac4C (#A18806 Abclonal, Woburn, MA, USA), anti-phosphorylated histone H2AX (γH2AX; phospho S139) (#05-636, Merck, Germany), anti-fibrillarin (#ab4566, Abcam), anti- phospho-ATM; Ser1981 (#MAB3806-C, Merck, Germany), anti-m6A (#202 111, SYSY Antibodies, Goettingen, Germany), and anti-NAT10 (B-4) (#sc-271770, Santa Cruz Biotechnology, Dallas, TX, USA). Second-day samples were washed twice in PBS for 15 min and incubated with the following secondary antibodies diluted at 1:300 in 1% BSAT: Alexa 488-conjugated goat anti-mouse (#ab150077, Abcam, UK), Alexa 594-conjugated goat anti-rabbit (#A11037, ThermoFisher Scientific, USA), Alexa 488-conjugated goat anti-mouse (#A11029, ThermoFisher Scientific, USA), Alexa Fluor 594-conjugated goat anti-mouse (#A11032, ThermoFisher Scientific, USA), and Alexa 647-conjugate goat anti-rabbit (#A21245, ThermoFisher Scientific). The DNA content was visualized using 4',6-diamidino-2-phenylindole (DAPI; Sigma-Aldrich, Germany), and Vectashield (Vector Laboratories, USA) was used as the mounting medium. Samples were also incubated without primary antibodies for negative control staining.

Local laser microirradiation and laser scanning confocal microscopy

For the micro irradiation experiments using UVA lasers (wavelength 355 nm), cells were seeded on 35 mm gridded microscope dishes (#81166, Ibidi, Fitchburg, WI, USA) and at 50% confluence were sensitized with 10 μM BrdU for 16 to 18 h. The cells were maintained under optimal cultivation conditions in an incubation chamber (EMBL) at 37°C with 5% CO2. In the selected cell nuclei, we irradiated only the defined region of interest (ROI) using a TCS SP5-X confocal microscope system (Leica, Wetzlar, Germany). The microscope settings for induction of local DNA damage were as follows: power laser (355 nm) 25 mW, 512×512 pixel resolution, 400 Hz, bidirectional mode, 48 lines, zoom 8 and 63x oil objective (HCX PL APO, lambda blue) with a numerical aperture (NA) = 1.4 [17]. The maximum observed irradiation

duration was 45 minutes, and for the data analysis, we monitored about 100 cell nuclei. The analysis of 3 biological replicates was performed. After the immunostaining procedure, locally micro-irradiated cells were found according to registered coordinates on gridded microscope dishes. We studied the level of the epigenetic marker N4-acetylcytidine in RNA, NAT 10 acetyltransferase, and the presence of γH2AX (phospho S139), which was also used for the optimization of micro irradiation experiments.

Images were acquired by laser scanning confocal microscopy (Leica TCS SP5-X or Leica SP-8 system). For observation and image acquisition, the following parameters were used: 1024 × 1024 pixels, 400 Hz, bidirectional scanning mode, 8 lines, zoom 5–8, and 63× oil objective (HCX PL APO, lambda blue) with a numerical aperture (NA) = 1.4. LEICA LAS X software was used for image acquisition and fluorescence intensity analysis.

Statistical analysis

Fluorescence intensity values were measured by LAS X software and subsequently analyzed in Python 3. The obtained data were compared statistically using the ANOVA One-Way test, available in GraphPad Prism software, version 9 for Windows (GraphPad Software, San Diego, CA, USA). All cases where $p \leq 0.05$ were considered statistically significant and are presented in graphs in the results section.

Results

ac4C RNAs recognizes UVA and UVC-induced DNA lesions

Local laser microirradiation showed that ac4C RNAs recruit to microirradiated chromatin immediately after genome injury. The ac4c RNA signal weakens 20-40 min post-irradiation (Fig. 1). In non-irradiated cells, we have observed that ac4C RNA occupies a compartment of nucleoli (Fig. 1), which was additionally verified by dual immunolabelling showing in parallel ac4 RNA and fibrillarin, a main component of nucleoli (Fig. 2A, B). The fibrillarin-positive region of nucleoli of non-irradiated cells was dense on ac4C RNA, and inhibitor of RNA polymerase I, actinomycin D, caused the so-called crescent-like morphology of the fibrillarin-positive region of nucleoli. Also, these crescents colocalized with ac4C RNAs (Fig. 2A). Ac4C RNAs recognized UVA-induced DNA lesions also when the cells were treated by actinomycin D (Fig. 2B).

When the cells were as the whole cell population irradiated by UVC lamp, we found a high density of ac4C RNA in the nucleoplasm of the cells exposed to UVC and analyzed 20 minutes post-irradiation. Cells analyzed 90-120 minutes after irradiation were characterized by ac4C RNA reorganization into well-visible, tiny foci (Fig. 3A-E). In such UVC-irradiated cells, we quantified ac4C RNA distribution in the whole nuclear content (Fig. 3B). As can be seen in Figures 3A and 3E, in non-irradiated cells, the most significant amount of ac4C RNA was concentrated in nucleoli; on the other hand, after UVC irradiation, the highest fluorescence intensity we observed in the nucleoplasm (3A-E). The ratio of the relative fluorescence intensities (FI) in the nucleus to the rest of FI of ac4C RNA in the nucleus was 2.42 (median) in the control cells. For irradiated samples, at intervals 5 min, 20 min, 50 min, and 120 min after irradiation, the FI range

was from 0.44 to 0.94 (on average). The difference in relative intensities was highly statistically significant ($p \leq 0.0001$) (Fig. 3E). The most marked changes in the nucleoplasm were detected 5 minutes after irradiation, then the amount of ac4C RNA decreased. Differences in absolute fluorescence intensity within the nucleus were statistically significant in all compared groups ($p \leq 0.0001$); (Fig. 3B, 3C). Interestingly, the total FI of fluorescently stained ac4C RNA in the nucleoli was significant after irradiation, and an increase in ac4C RNA inside the nucleoli was also 120 min after irradiation, but the trend in the nucleoplasm was the opposite (Fig. 3D, 3E). These results suggest that UV radiation increases the acetylation of N4-cytidine in nucleoplasmic RNAs.

Accumulation of ac4C RNA in DNA lesions is PARP dependent

We have addressed the question if a pronounced appearance of ac4C at DNA lesions is PARP-dependent. We treated the cells with a PARP inhibitor, olaparib. In non-irradiated cells, we have observed a high density of ac4 RNA in nucleoli, 10 min after UVA irradiation, a high level of ac4 RNAs was detected in the nucleoplasm, while the cells treated by PARP inhibitor were characterized by the identical distribution profile fo ac4C RNA as in control non-irradiated cells (Fig. 4A). PARP inhibitor olaparib also prevents the recruitment of ac4C RNA to UVA-microirradiated chromatin; thus, these data show that accumulation of ac4C RNAs to locally-induced DNA is PARP-dependent (Fig. 4B).

Recruitment of ac4C at UVA-damaged chromatin is not dependent on the function of NAT10 acetyltransferase

It is well-known that RNA cytidine acetyltransferase NAT10 is responsible for the installation of N4-acetylcytidine (ac4C) on mRNAs, 18S rRNA, and tRNAs [13, 14]. It was observed that NAT10 is responsible for the formation of ac4C at position 1842 in 18S rRNA [13]. Based on this information, we analyzed if recruitment of ac4C RNA to DNA lesions is NAT10 depend. In this case, we found that NAT10 is not recruited to microirradiated chromatin; thus, it seems likely that ac4C installation on RNA at UV-induced DNA lesions is not mediated via NAT10 acetyltransferase (Fig. 5).

Here, we also compare ac4C RNA accumulation at microirradiated chromatin with m^6A RNA appearance at DNA lesions, as we studied recently [17]. We found distinct recruitment kinetics for ac4C RNAs and m^6A RNAs at DNA lesions. In general, a peak of accumulation is identical for both ac4C RNAs and m^6A RNAs, but a high level of ac4C RNAs at microirradiated chromatin remains longer, up to 30-45 min postirradiation, in comparison to m^6A RNAs (Fig. 6).

An increase in ac4C RNA level after UV irradiation is identical in all phases of the interphase.

For such experiments, we used HeLa-Fucci cells expressing RFP-Cdt1 in the G1 phase and GFP-tagged geminin in the G2 phase of the cell cycle [20]. In G1, S, and G2 cell cycle phases, we observed an identical increase in ac4C RNA level when the whole cell population was irradiated by UV light and compared with non-irradiated cells (Fig. 7A, B).

Discussion

Acetylation processes and their regulation via specific epigenetic writes (acetyltransferases) and erasers (deacetylases) are well-described on histones. Another component of chromatin, which is DNA, is absent of acetylation marks, but in distinct types of RNAs, acetylation of N4-cytidine (ac4C) was described as a unique regulatory factor that originates from epitranscriptome [25]. From the view of nucleic acid biology and chromatin features, ac4C on RNAs is a unique biochemical event. It is known that RNA can be acetylated on cytidine via a specific RNA acetyltransferase, called NAT10, and ac4C on RNA can be erased via the function of sirtuin 7 [15]. Thus, these important factors of RNA biology we studied in this paper showing NAT10-independent recruitment of ac4C RNA to UV-induced DNA lesions.

It is well-known that RNA can also be methylated on adenosine (m^6A), which regulates many biological processes, including transcription, translation, RNA stability, and also DNA repair [16, 17]. From the view of DNA damage repair processes, Yang et al. (2017) [16] showed that m^6A RNA participates in DNA damage response. Moreover, Zhang et al. (2017) [18] suggested the existence of a non-canonical and PARP-dependent DNA repair pathway which function is based on m^6A RNAs that recognize UV-induced DNA lesions. A very important is also a discovery of hybrid DNA/m^6A-modified RNA loops maintaining physiological processes in the genome after injury. It was documented that DNA- RNA hybrid loops and R-loops at the sites of the DNA break have both positive and negative roles in homology-directed recombination repair (HRR) [26–30]. In our case, we have observed that these hybrid loops are rather involved in a base excision repair (BER) mechanism because the protein of BER, XRCC1, behaves identically at DNA lesions as another RNA modification 8-adenosine methylation (m^8A) that also recognized microirradiated chromatin [31]. Notably, both XRCC1 and m^8A RNAs were not detected at microirradiated genomic regions when the cells were treated by PARP inhibitor [31]. Based on these results, we have continued with the analysis of RNA modifications at DNA lesions. We addressed the question of also ac4C RNAs recognize locally micro-irradiated chromatin. Indeed, a high level of ac4C RNA we observed at irradiated genomic regions by UVA laser (Fig. 1). Also, UVC-light causes elevation of ac4C RNA level in the whole cell nuclei (Fig. 3A). Importantly, similarly to m^6A RNAs and m^8A RNAs, ac4C RNAs were accumulated to microirradiated genomic regions, and this process was PARP dependent [18, 31] (Fig. 4A, B). A very interesting is observation that the kinetics of ac4C RNAs at the lesions is different from the kinetics of m^6A RNAs at microirradiated chromatin (Fig. 6 and [17]). Also, all studied RNA modifications were recruited to DNA lesions independently of the cell cycle, as we analyzed in HeLa Fucci cellular system ([31]; Fig. 7). As mentioned above, in Legartová et al. preprint (2021) [31], we show that m^8A RNAs likely contribute to the BER repair mechanism. Moreover, a high degree of interaction we have also found between m^8A RNAs and γH2AX or m^8A RNAs and DNA. From this view, it seems to be likely γH2AX stabilizes hybrid DNA-RNA structures that appear around DNA lesions. Also, our observation fits well with the theory of PARP-dependent DNA repair pathway(s), in which co-transcriptionally modified RNAs are key players.

Declarations

Conflict of Interest: We declare no conflict of interest

Author Contributions:

AK was responsible for immunofluorescence, laser microirradiation, and data analysis. AK supports experimental models. LS cultivated cells and optimized microirradiation protocol. EB suggested experimental design, wrote the paper, and finalized images. All authors have read and agreed to publish this preprint version of the manuscript.

Funding

Experiments were funded by the internal support of the Institute of Biophysics and the Strategy of the Czech Academy of Sciences (IC68081707).

References

1. Bannister, A.J. and Kouzarides, T. Regulation of chromatin by histone modifications. *Cell Research* 2011 21, 381–395. 10.1038/cr.2011.22
2. Arango, D. *et al.* Acetylation of Cytidine in mRNA Promotes Translation Efficiency. *Cell* 2018 175, 1872-1886.e1824. 10.1016/j.cell.2018.10.030
3. Tjeertes, J.V., Miller, K.M. and Jackson, S.P. Screen for DNA-damage-responsive histone modifications identifies H3K9Ac and H3K56Ac in human cells. *Embo j* **2009** 28, 1878–1889. 10.1038/emboj.2009.119
4. Sustáčková, G. *et al.* Acetylation-dependent nuclear arrangement and recruitment of BMI1 protein to UV-damaged chromatin. *J Cell Physiol* **2012** 227, 1838–1850. 10.1002/jcp.22912
5. Meyer, B. *et al.* Histone H3 Lysine 9 Acetylation Obstructs ATM Activation and Promotes Ionizing Radiation Sensitivity in Normal Stem Cells. *Stem Cell Reports* **2016** 7, 1013–1022. 10.1016/j.stemcr.2016.11.004
6. Dhar, S., Gursoy-Yuzugullu, O., Parasuram, R. and Price, B.D. The tale of a tail: histone H4 acetylation and the repair of DNA breaks. *Philosophical Transactions of the Royal Society B: Biological Sciences* **2017** 372, 20160284. 10.1098/rstb.2016.0284
7. Gong, F. *et al.* Screen identifies bromodomain protein ZMYND8 in chromatin recognition of transcription-associated DNA damage that promotes homologous recombination. *Genes Dev* **2015** 29, 197–211. 10.1101/gad.252189.114
8. Gursoy-Yuzugullu, O., Carman, C. and Price, B. Spatially restricted loading of BRD2 at DNA double-strand breaks protects H4 acetylation domains and promotes DNA repair. *Scientific Reports* **2017** 7. 10.1038/s41598-017-13036-5
9. Jacquet, K. *et al.* The TIP60 Complex Regulates Bivalent Chromatin Recognition by 53BP1 through Direct H4K20me Binding and H2AK15 Acetylation. *Mol Cell* **2016** 62, 409–421. 10.1016/j.molcel.2016.03.031

10. Xu, Y. *et al.* The p400 ATPase regulates nucleosome stability and chromatin ubiquitination during DNA repair. *J Cell Biol* 2010 191, 31–43. 10.1083/jcb.201001160
11. Gursoy-Yuzugullu, O., Ayrapetov, M.K. and Price, BD. Histone chaperone Anp32e removes H2A.Z from DNA double-strand breaks and promotes nucleosome reorganization and DNA repair. *Proc Natl Acad Sci U S A* 2015 112, 7507–7512. 10.1073/pnas.1504868112
12. Thomas, J.M. *et al.* A Chemical Signature for Cytidine Acetylation in RNA. *J Am Chem Soc* **2018** 140, 12667–12670. 10.1021/jacs.8b06636
13. Ito, S. *et al.* Human NAT10 is an ATP-dependent RNA acetyltransferase responsible for N4-acetylcytidine formation in 18 S ribosomal RNA (rRNA). *J Biol Chem* **2014** 289, 35724–35730. 10.1074/jbc.C114.602698
14. Sharma, S. *et al.* Yeast Kre33 and human NAT10 are conserved 18S rRNA cytosine acetyltransferases that modify tRNAs assisted by the adaptor Tan1/THUMPD1. *Nucleic Acids Res* 2015 43, 2242–2258. 10.1093/nar/gkv075
15. Kudrin, P., Meierhofer, D., Vågbø, C.B. and Ørom, U.A.V. Nuclear RNA-acetylation can be erased by the deacetylase SIRT7. *bioRxiv* 2021 10.1101/2021.04.06.438707, 2021.2004.2006.438707. 10.1101/2021.04.06.438707
16. Xiang, Y. *et al.* RNA m6A methylation regulates the ultraviolet-induced DNA damage response. *Nature* **2017** 543, 573–576. 10.1038/nature21671
17. Svobodová Kovaříková, A. *et al.* N(6)-Adenosine Methylation in RNA and a Reduced m(3)G/TMG Level in Non-Coding RNAs Appear at Microirradiation-Induced DNA Lesions. *Cells* **2020** 9. 10.3390/cells9020360
18. Zhang, J. Brothers in arms: emerging roles of RNA epigenetics in DNA damage repair. *Cell & Bioscience* **2017** 7, 24. 10.1186/s13578-017-0151-9
19. Qu, F., Tsegay, P.S. and Liu, Y. N(6)-Methyladenosine, DNA Repair, and Genome Stability. *Front Mol Biosci* **2021** 8, 645823. 10.3389/fmolb.2021.645823
20. Sakaue-Sawano, A. *et al.* Visualizing Spatiotemporal Dynamics of Multicellular Cell-Cycle Progression. *Cell* **2008** 132, 487–498. 10.1016/j.cell.2007.12.033
21. Park, H.J. *et al.* The PARP inhibitor olaparib potentiates the effect of the DNA damaging agent doxorubicin in osteosarcoma. *Journal of Experimental & Clinical Cancer Research* **2018** 37, 107. 10.1186/s13046-018-0772-9
22. Stixová, L. *et al.* Localization of METTL16 at the Nuclear Periphery and the Nucleolus Is Cell Cycle-Specific and METTL16 Interacts with Several Nucleolar Proteins. *Life (Basel)* 2021 11. 10.3390/life11070669
23. Hahn, P. *et al.* Analysis of Jmjd6 Cellular Localization and Testing for Its Involvement in Histone Demethylation. *PLOS ONE* 2010 5, e13769. 10.1371/journal.pone.0013769
24. Svobodová Kovaříková, A., Legartová, S., Krejčí, J. and Bártová, E. H3K9me3 and H4K20me3 represent the epigenetic landscape for 53BP1 binding to DNA lesions. *Aging (Albany NY)* 2018 10, 2585–2605. 10.18632/aging.101572

25. Zhao, W., Zhou, Y., Cui, Q. and Zhou, Y. PACES: prediction of N4-acetylcytidine (ac4C) modification sites in mRNA. *Scientific Reports* **2019** 9, 11112. 10.1038/s41598-019-47594-7
26. Ohle, C. *et al.* Transient RNA-DNA Hybrids Are Required for Efficient Double-Strand Break Repair. *Cell* 2016 167, 1001-1013.e1007. 10.1016/j.cell.2016.10.001
27. Cohen, S. *et al.* Senataxin resolves RNA:DNA hybrids forming at DNA double-strand breaks to prevent translocations. *Nature Communications* **2018** 9, 533. 10.1038/s41467-018-02894-w
28. Costantino, L. and Koshland, D. Genome-wide Map of R-Loop-Induced Damage Reveals How a Subset of R-Loops Contributes to Genomic Instability. *Mol Cell* **2018** 71, 487-497.e483. 10.1016/j.molcel.2018.06.037
29. García-Muse, T. and Aguilera, A. R Loops: From Physiological to Pathological Roles. *Cell* 2019 179, 604-618. 10.1016/j.cell.2019.08.055
30. Domingo-Prim, J., Bonath, F. and Visa, N. RNA at DNA Double-Strand Breaks: The Challenge of Dealing with DNA:RNA Hybrids. *BioEssays* **2020** 42, 1900225. https://doi.org/10.1002/bies.201900225
31. Legartova Sona, S.J., Bartova Eva (2021). PARP dependent recruitment of RNA methylated at 8-adenosine is linked to base excision repair mechanism. Research Sqaure, DOI: https://doi.org/10.21203/rs.3.rs-892499/v1

Figures

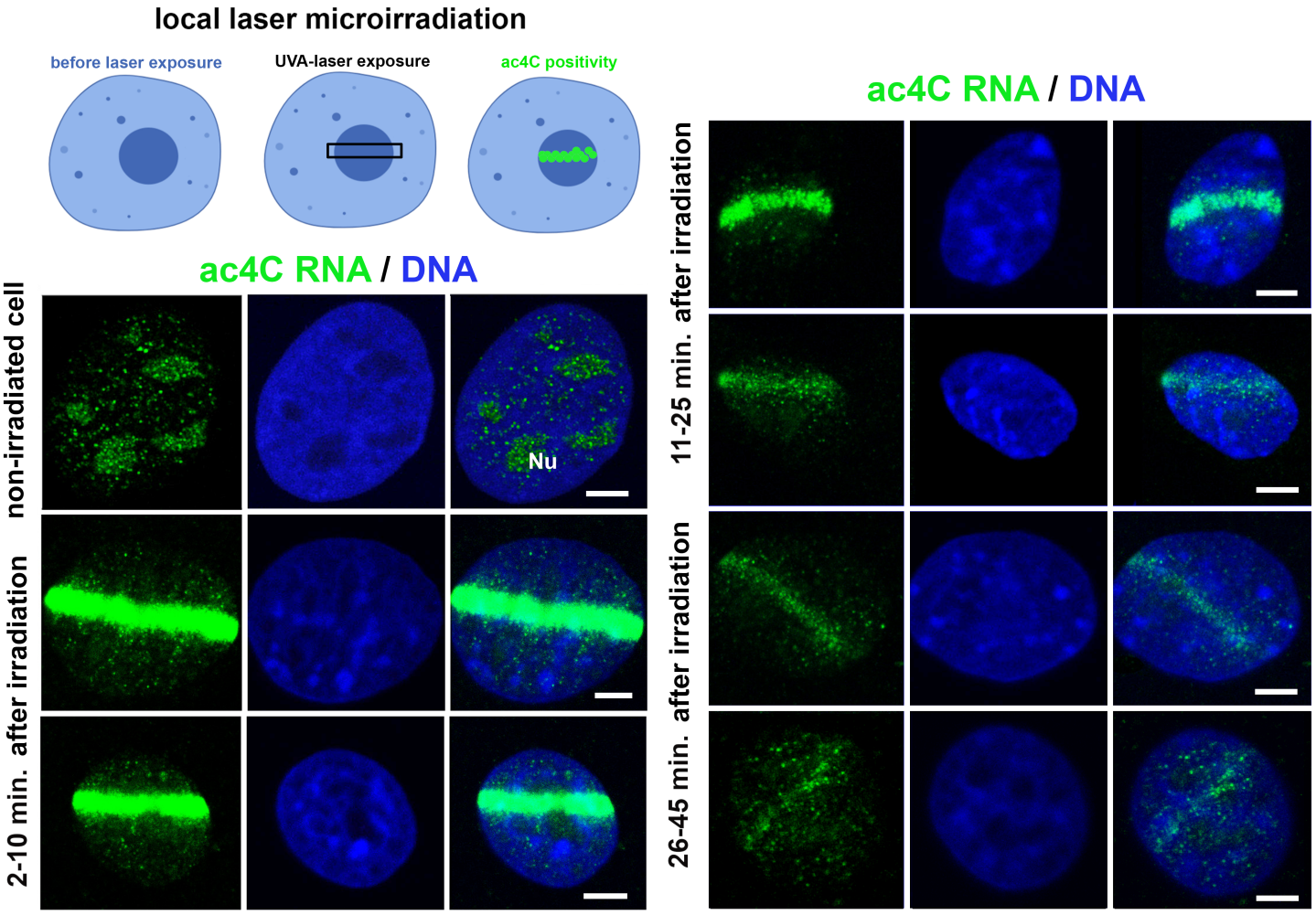

Figure 1

Recruitment of ac4C RNAs at UVA-damaged chromatin. Local laser microirradiation showed that ac4C RNAs recognized UVA-microirradiated chromatin immediately after local laser irradiation. In later stages of DDR, 25-40 min post-irradiation, the ac4C RNA signal at DNA lesions disappeared. Scale bars showed 5 μm.

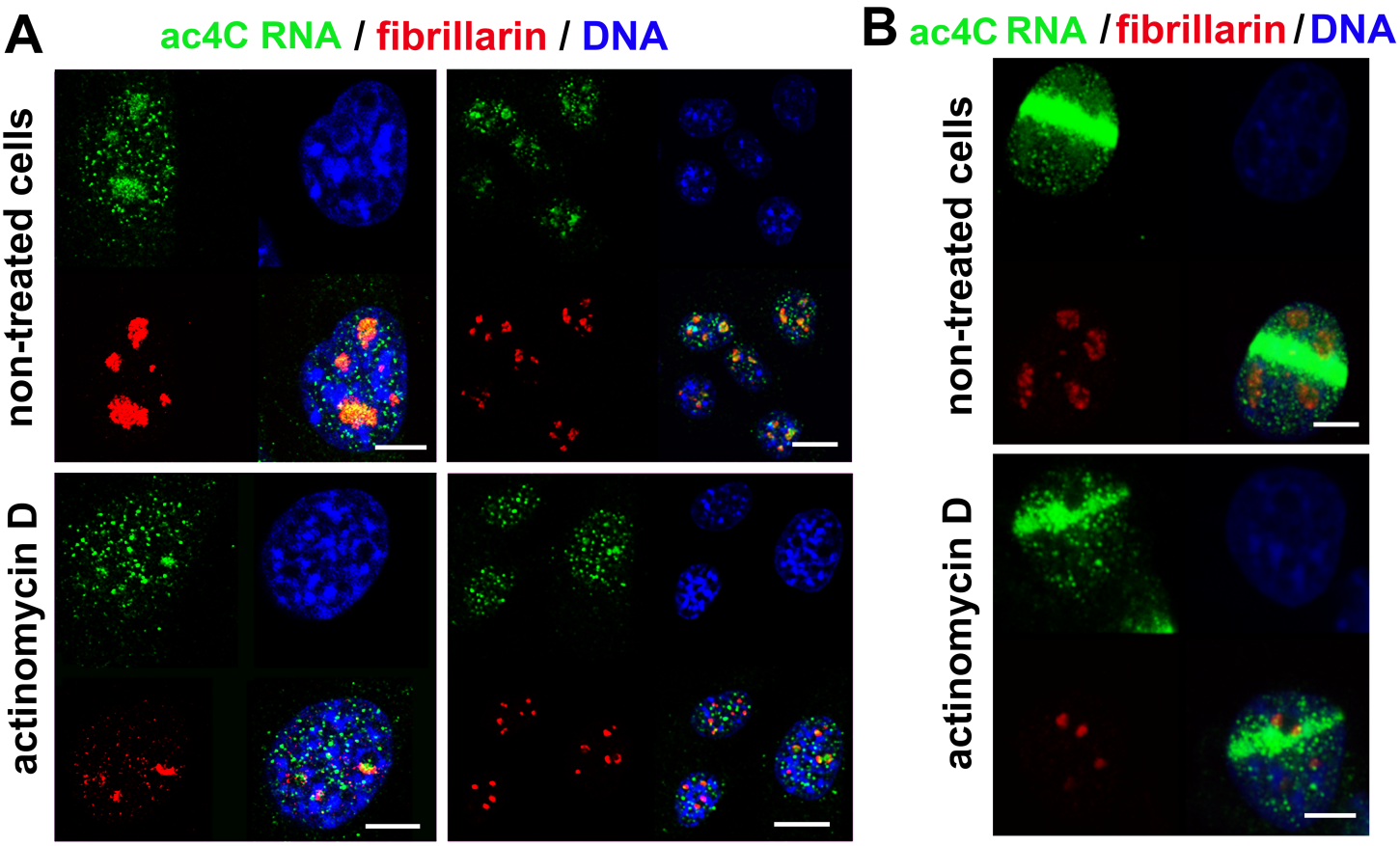

Figure 2

A high density of ac4C RNA is inside nucleoli. (A-B) Ac4C RNAs colocalized with fibrillarin-positive regions of nucleoli. The same nuclear distribution profile was observed in MEFs treated by actinomycin D, an inhibitor of RNA pol I. Scale bars showed 5 μm.

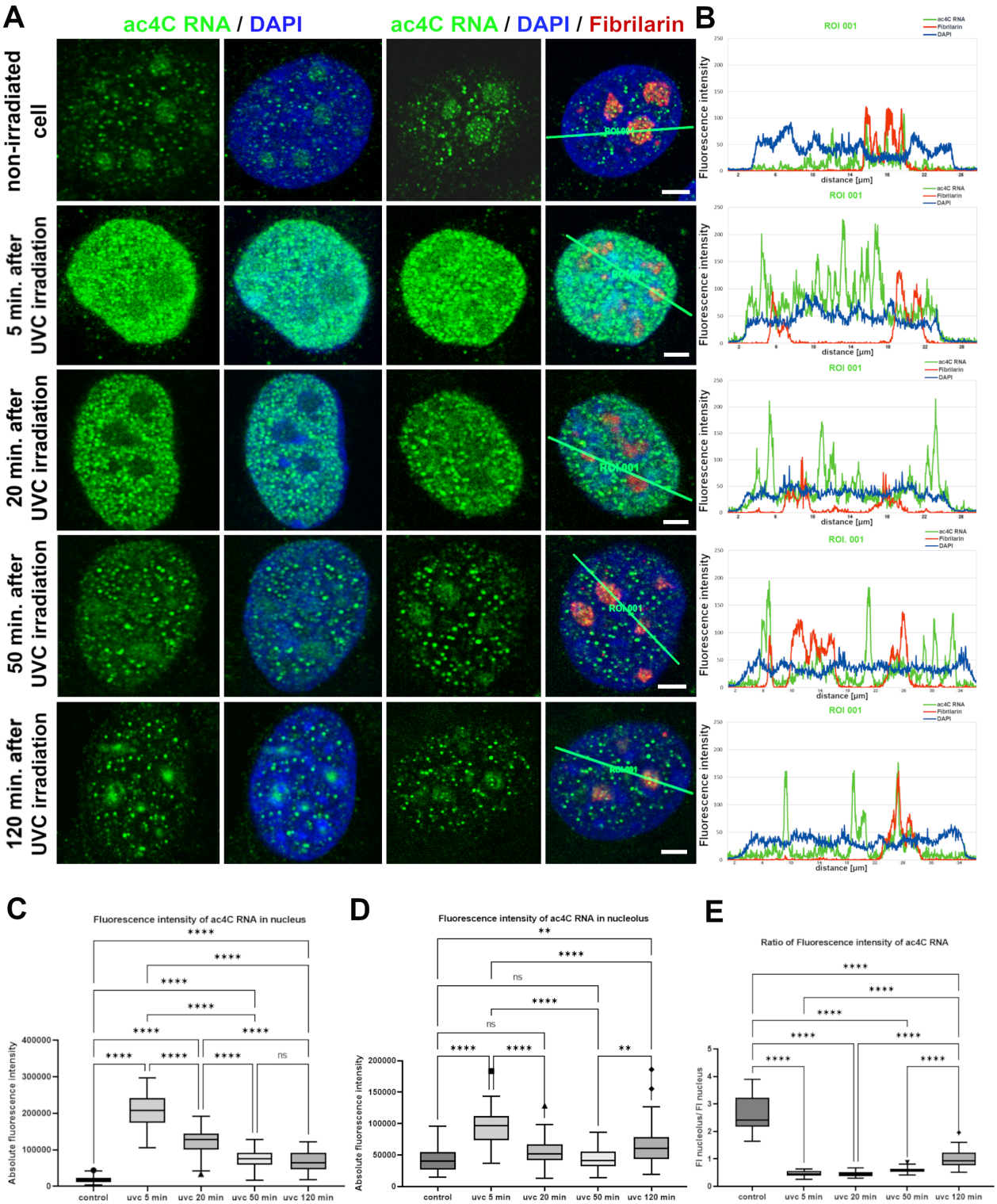

Figure 3

UVC light caused an accumulation of ac4C RNA into well-visible foci in a later stage of DDR. (A) In non-irradiated control cells, relatively high ac4C RNA positivity was observed in nucleoli (detected using fibrillarin immunostaining). UVC irradiation increased the level of ac4C RNA in the nucleoplasm, 20 min postirradiation, while MEFs analyzed 20-120 minutes after UVC-irradiation were characterized by ac4C RNA reorganization into well-visible and ac4C dense foci. Scale bars showed 5 µm. (B) Quantification

shows the fluorescent intensity (FI) of ac4c RNA in the nucleoplasm (green), compared with fibrillarin-positive regions of nucleoli (red) and DAPI-stained DNA (blue). (C) Box plot graphs display the absolute intensity of ac4C RNA in the nucleoplasm. (D) Box plot graphs show the total intensity of fluorescently-stained ac4C RNA in nucleoli. (E) Box plot graphs depict the fluorescent intensity ratio of ac4C RNA occupying nucleoli and the nucleoplasm.

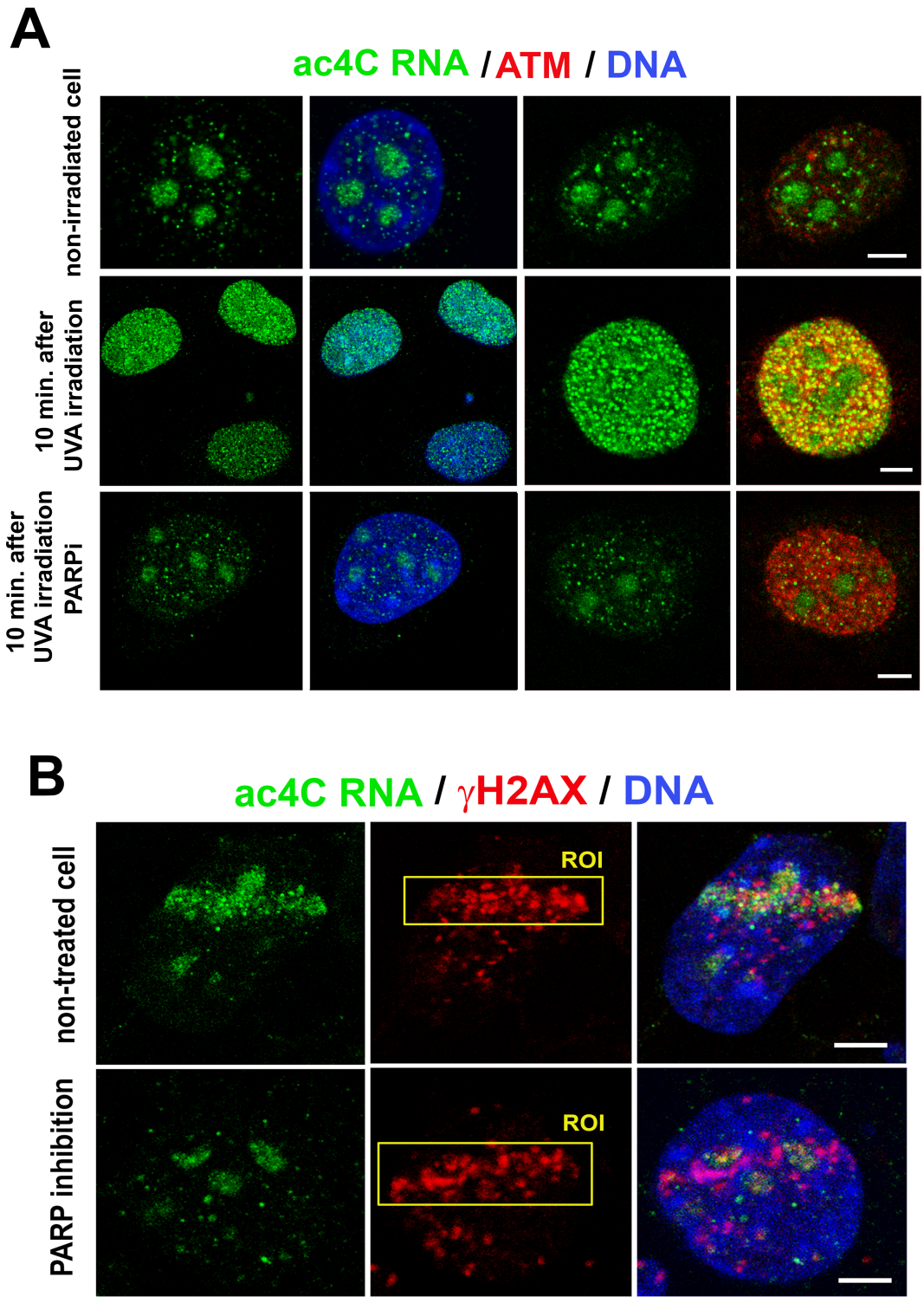

Figure 4

PARP-dependent recruitment of ac4C to UVA-damaged chromatin. Local laser microirradiation showed that ac4C RNAs did not accumulate to DNA lesions when the cells were treated by PARP inhibitor. It was observed in both (A) UVA irradiated MEFs as a whole-cell population and (B) microirradiated MEFs by UVA laser. Scale bars showed 5 μm.

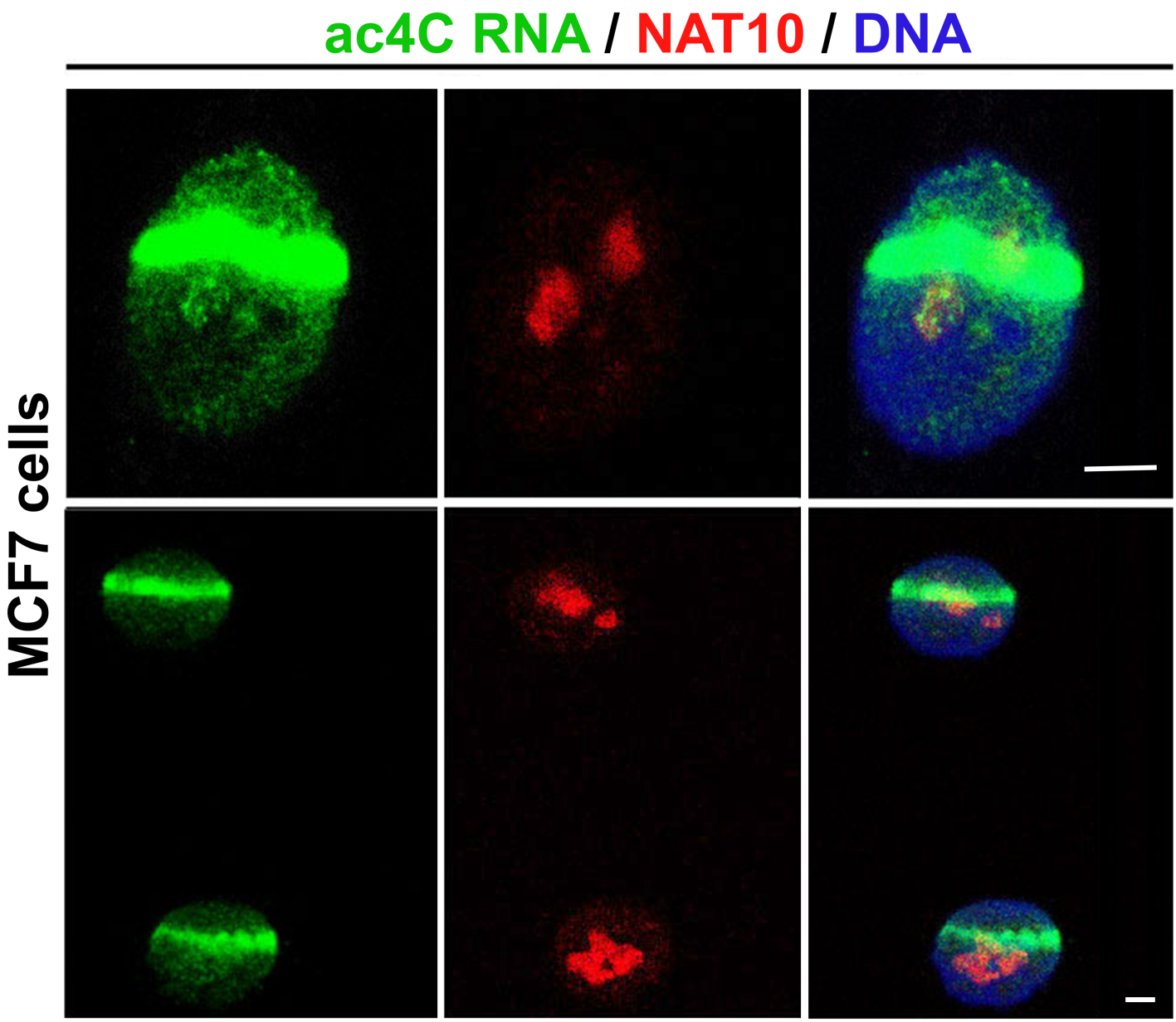

Figure 5

NAT10-independent recruitment of ac4C RNA to UVA-damaged chromatin. Local laser microirradiation showed that NAT10 acetyltransferase (red) does not recruit to DNA lesions (positive on ac4C RNA; green) induced in MCF7 cells. These cells were studied instead of MEFs due to antibody availability. Scale bars showed 5 μm.

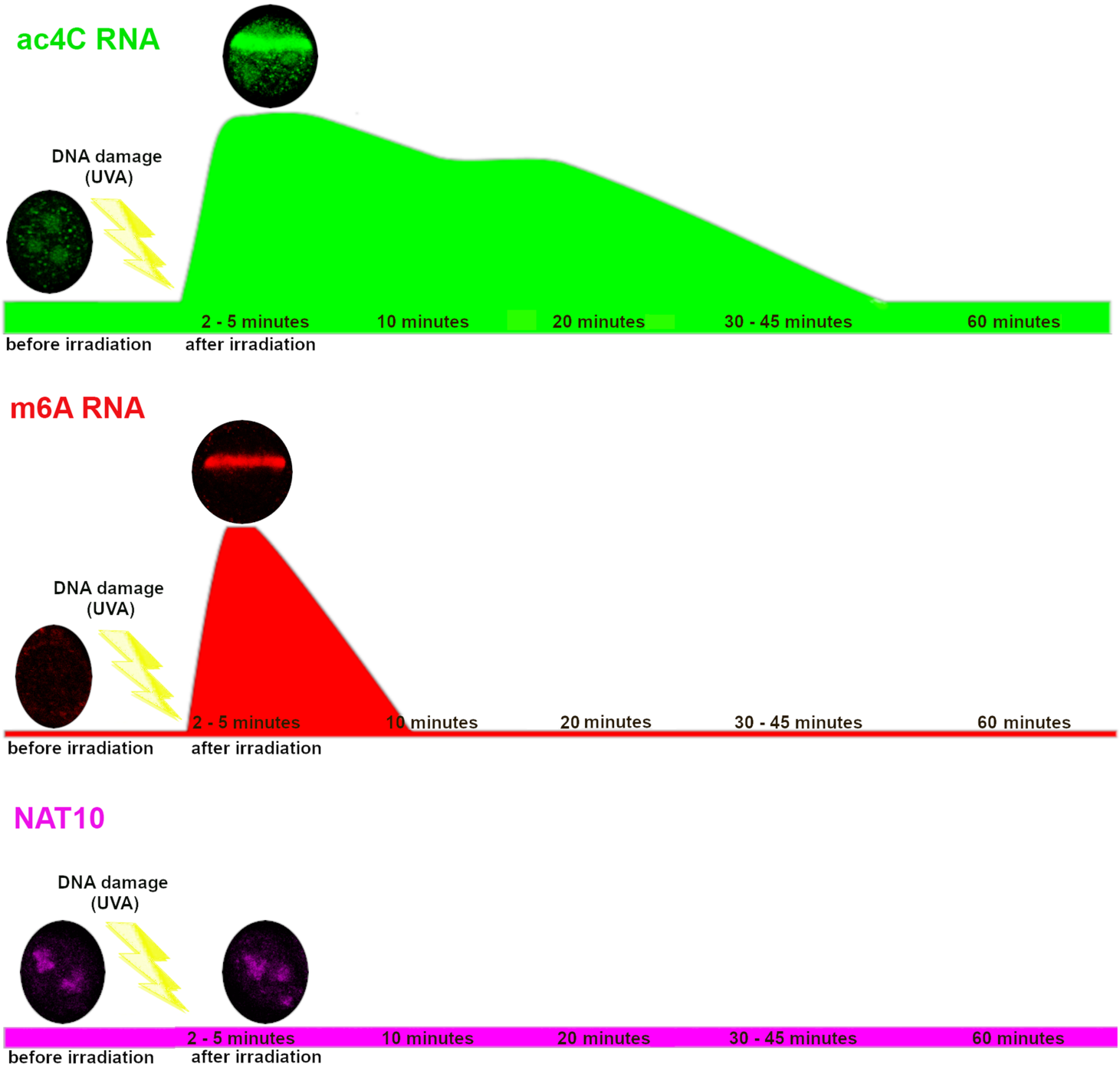

Figure 6

Distinct kinetics of ac4C RNAs and m6A RNA at DNA lesions. The pictorial illustration shows distinctions in ac4C RNA recruitment to microirradiated chromatin compared to m6A RNAs accumulation at laser-induced DNA lesions. Ac4C RNA recruitment to microirradiated chromatin was NAT10 independent.

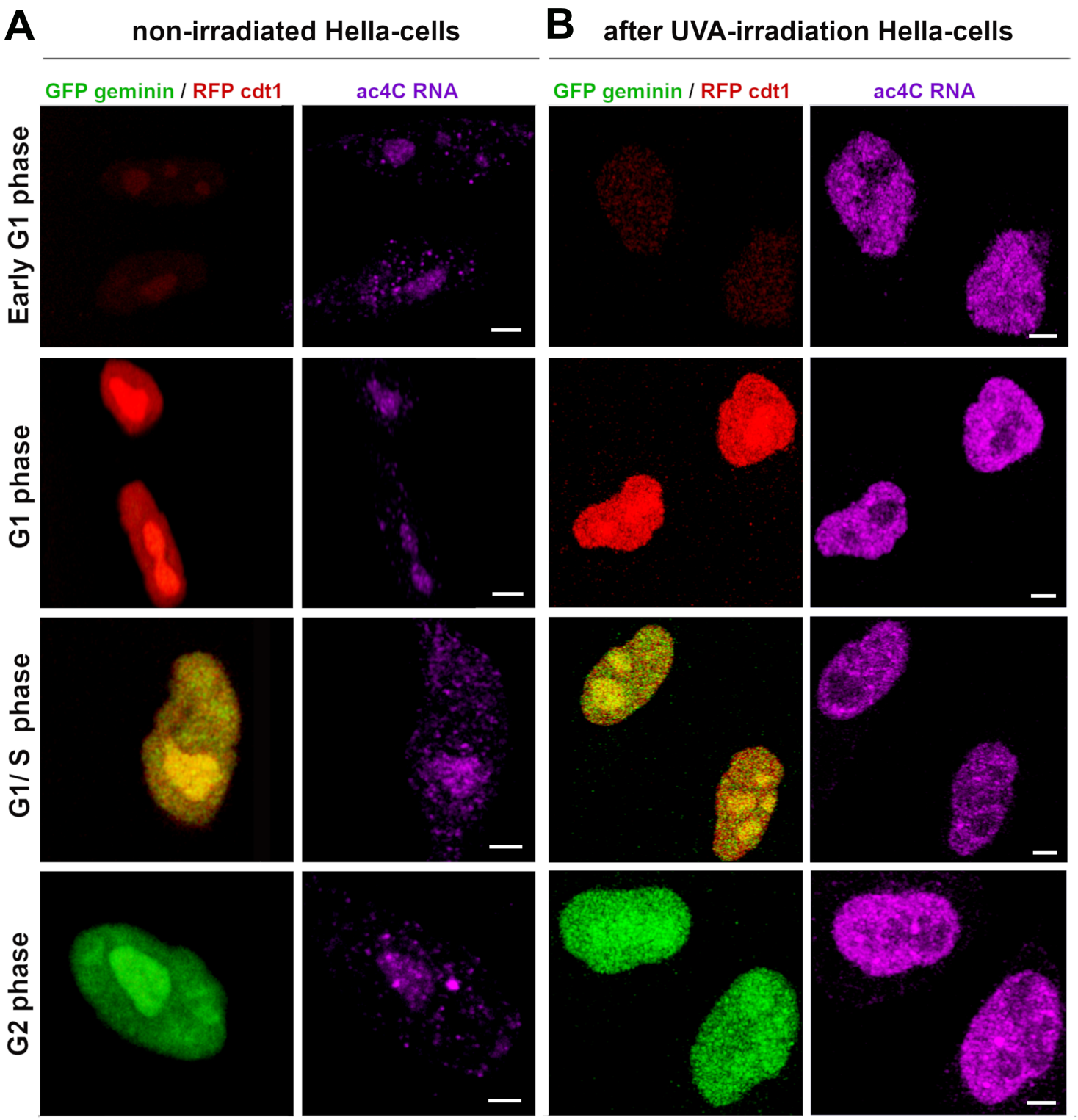

Figure 7

Increased levels of ac4C RNAs after UV irradiation are identical in the G1, S, and G2 phases of the cell cycle. The density of ac4C RNA was detected in (A) in non-irradiated Fucci cells and (B) UV-irradiated Fucci cells, stably expressing cdt1 (red) in the G1 phase and geminin (green) in the G2 phase of the cell cycle. S phase is characterized by a weak cdt1 and geminin positivity. Scale bars show 5 mm.